

# Overview

---

## Past work

Soil Desiccation

Intergranular Fracture in UO<sub>2</sub>

## Preliminary results and findings

Towards ductile fracture

## References

Past work

Soil Desiccation

Intergranular Fracture in UO<sub>2</sub>

Preliminary results and findings

Towards ductile fracture

References

Past work

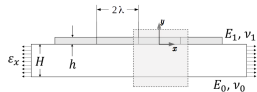
Soil Desiccation

Intergranular Fracture in UO<sub>2</sub>

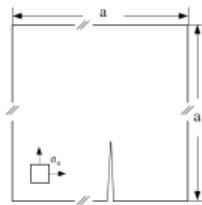
Preliminary results and findings

Towards ductile fracture

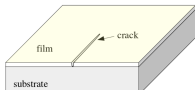
References



(a)



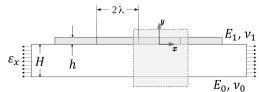
(b)



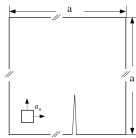
(c)

- ▶ Only “channeling” cracks in the thin film are considered.
- ▶ Small deformation is assumed for  $\pi_{\text{elastic}}$ , and  $\boldsymbol{\varepsilon} = (\nabla \mathbf{u} + \nabla^T \mathbf{u})/2$ .
- ▶ A frictionless contact split of the elastic energy is applied at the vicinity of the crack set.
- ▶ Thermal effects are neglected. Dehydration is modeled as pre-stress in  $\pi_{\text{inelastic}} = \sigma_0 \text{tr}(\boldsymbol{\varepsilon})$ .
- ▶ A cohesive-type fracture model is used for  $\pi_{\text{fracture}}$ .

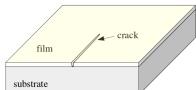
See mud.pdf for details.



(a)



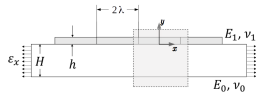
(b)



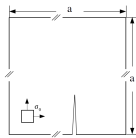
(c)

- ▶ Only “channeling” cracks in the thin film are considered.
- ▶ Small deformation is assumed for  $\pi_{\text{elastic}}$ , and  $\boldsymbol{\varepsilon} = (\nabla \mathbf{u} + \nabla^T \mathbf{u})/2$ .
- ▶ A frictionless contact split of the elastic energy is applied at the vicinity of the crack set.
- ▶ Thermal effects are neglected. Dehydration is modeled as pre-stress in  $\pi_{\text{inelastic}} = \sigma_0 \text{tr}(\boldsymbol{\varepsilon})$ .
- ▶ A cohesive-type fracture model is used for  $\pi_{\text{fracture}}$ .
- ▶ The model is verified with analytical solutions in a periodic quasi-1D context (Fig. a).

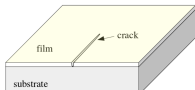
See mud.pdf for details.



(a)



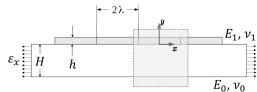
(b)



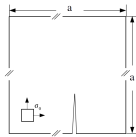
(c)

- ▶ Only “channeling” cracks in the thin film are considered.
- ▶ Small deformation is assumed for  $\pi_{\text{elastic}}$ , and  $\boldsymbol{\varepsilon} = (\nabla \mathbf{u} + \nabla^T \mathbf{u})/2$ .
- ▶ A frictionless contact split of the elastic energy is applied at the vicinity of the crack set.
- ▶ Thermal effects are neglected. Dehydration is modeled as pre-stress in  $\pi_{\text{inelastic}} = \sigma_0 \text{tr}(\boldsymbol{\varepsilon})$ .
- ▶ A cohesive-type fracture model is used for  $\pi_{\text{fracture}}$ .
- ▶ The model is verified with analytical solutions in a periodic quasi-1D context (Fig. a).
- ▶ Pervasive fracture is studied with a 2D simplification (Fig. b).
- ▶ The energy  $\pi_{\text{interface}}$  accounts for mismatch between the film and the substrate.
- ▶ Material property inhomogeneity in the macroscopic continuum model is taken into account by introducing two pointwise correlated random fields  $\{\mathcal{G}_c(\mathbf{X}), \mathbf{X} \in \Omega\}$  and  $\{\pi_c(\mathbf{X}), \mathbf{X} \in \Omega\}$ .

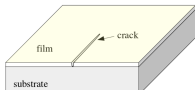
See [mud.pdf](#) for details.



(a)



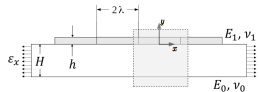
(b)



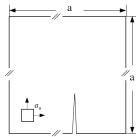
(c)

See [mud.pdf](#) for details.

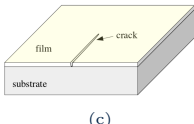
- ▶ Only “channeling” cracks in the thin film are considered.
- ▶ Small deformation is assumed for  $\pi_{\text{elastic}}$ , and  $\boldsymbol{\varepsilon} = (\nabla \mathbf{u} + \nabla^T \mathbf{u})/2$ .
- ▶ A frictionless contact split of the elastic energy is applied at the vicinity of the crack set.
- ▶ Thermal effects are neglected. Dehydration is modeled as pre-stress in  $\pi_{\text{inelastic}} = \sigma_0 \text{tr}(\boldsymbol{\varepsilon})$ .
- ▶ A cohesive-type fracture model is used for  $\pi_{\text{fracture}}$ .
- ▶ The model is verified with analytical solutions in a periodic quasi-1D context (Fig. a).
- ▶ Pervasive fracture is studied with a 2D simplification (Fig. b).
- ▶ The energy  $\pi_{\text{interface}}$  accounts for mismatch between the film and the substrate.
- ▶ Material property inhomogeneity in the macroscopic continuum model is taken into account by introducing two pointwise correlated random fields  $\{\mathcal{G}_c(\mathbf{X}), \mathbf{X} \in \Omega\}$  and  $\{\pi_c(\mathbf{X}), \mathbf{X} \in \Omega\}$ .
- ▶ The versatility offered by the probabilistic framework is highlighted by solving a 3D problem based on physical experiments.



(a)



(b)



(c)

See [mud.pdf](#) for details.

- ▶ Only “channeling” cracks in the thin film are considered.
- ▶ Small deformation is assumed for  $\pi_{\text{elastic}}$ , and  $\epsilon = (\nabla \mathbf{u} + \nabla^T \mathbf{u})/2$ .
- ▶ A frictionless contact split of the elastic energy is applied at the vicinity of the crack set.
- ▶ Thermal effects are neglected. Dehydration is modeled as pre-stress in  $\pi_{\text{inelastic}} = \sigma_0 \text{tr}(\epsilon)$ .
- ▶ A cohesive-type fracture model is used for  $\pi_{\text{fracture}}$ .
- ▶ The model is verified with analytical solutions in a periodic quasi-1D context (Fig. a).
- ▶ Pervasive fracture is studied with a 2D simplification (Fig. b).
- ▶ The energy  $\pi_{\text{interface}}$  accounts for mismatch between the film and the substrate.
- ▶ Material property inhomogeneity in the macroscopic continuum model is taken into account by introducing two pointwise correlated random fields  $\{\mathcal{G}_c(\mathbf{X}), \mathbf{X} \in \Omega\}$  and  $\{\pi_c(\mathbf{X}), \mathbf{X} \in \Omega\}$ .
- ▶ The versatility offered by the probabilistic framework is highlighted by solving a 3D problem based on physical experiments.

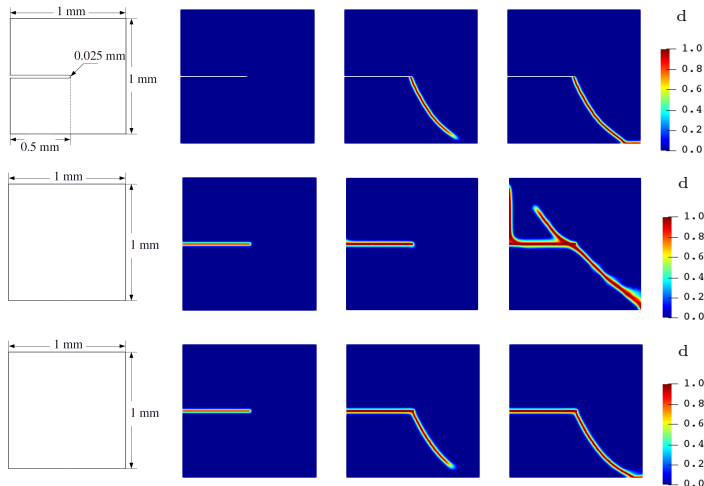
### The contact split

The elastic energy takes into account the tension-compression asymmetry and the frictionless contact condition at the vicinity of the crack set:

$$\pi_{\text{elastic}} = g_{qq}(d; p)\pi_{\text{elastic}}^{\langle A \rangle} + \pi_{\text{elastic}}^{\langle I \rangle}, \quad (1a)$$

$$\pi_{\text{elastic}}^{\langle A \rangle} = \begin{cases} \frac{1}{2}\lambda_s \langle \text{tr}(\boldsymbol{\varepsilon}) \rangle_+^2 + \mu_s \boldsymbol{\varepsilon}^+ : \boldsymbol{\varepsilon}^+, & d \leq d_{\text{critical}}, \\ \frac{1}{2}(\boldsymbol{\sigma}_n^+ + \boldsymbol{\sigma}_t) : \boldsymbol{\varepsilon}, & d > d_{\text{critical}}, \end{cases} \quad (1b)$$

$$\pi_{\text{elastic}}^{\langle I \rangle} = \begin{cases} \frac{1}{2}\lambda_s \langle \text{tr}(\boldsymbol{\varepsilon}) \rangle_-^2 + \mu_s \boldsymbol{\varepsilon}^- : \boldsymbol{\varepsilon}^-, & d \leq d_{\text{critical}}, \\ \frac{1}{2}\boldsymbol{\sigma}_n^- : \boldsymbol{\varepsilon}, & d > d_{\text{critical}}, \end{cases} \quad (1c)$$



The crack paths obtained using (1st row) the spectral decomposition on a geometrically notched plate, (2nd row) the spectral decomposition with an initial damage field, (3rd row) the contact split with an initial damage field.

Snapshots of crack paths are shown at (2nd column)  $u_x = 0 \text{ mm}$ , (3rd column)  $u_x = 0.0109 \text{ mm}$ , (4th column)  $u_x = 0.02 \text{ mm}$ .

### Material inhomogeneity

The covariance function  $\tau \mapsto R(\tau)$  for a  $[0, L]^n$   $p$ -periodic domain is given by

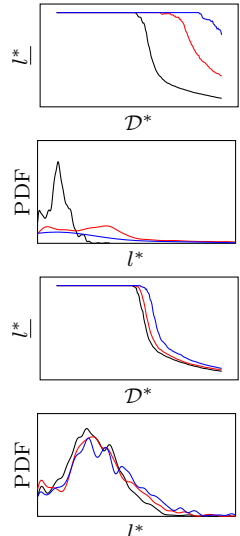
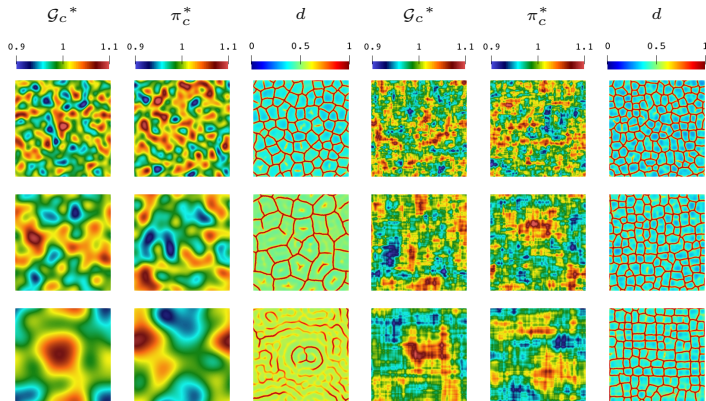
$$R(\tau) = \begin{bmatrix} R_1(\tau) & \rho R_1(\tau) \\ \rho R_1(\tau) & \rho^2 R_1(\tau) + (1 - \rho^2) R_2(\tau) \end{bmatrix}, \quad \forall \tau \in [0, p], \rho \in [-1, 1], \quad (2)$$

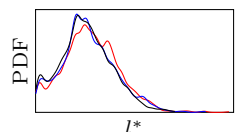
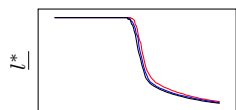
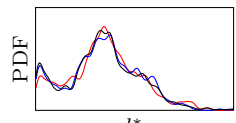
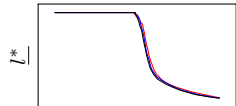
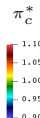
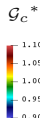
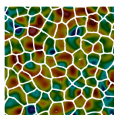
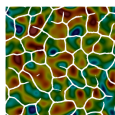
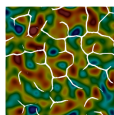
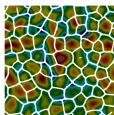
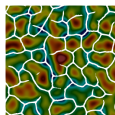
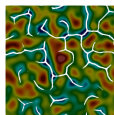
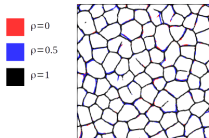
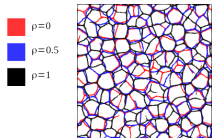
where the univariate covariance function  $R$  is assumed to take the generic form

$$R_\phi(\tau; L) = \exp(-c\phi(\tau; L)), \quad \forall \tau \in [0, p]. \quad (3)$$

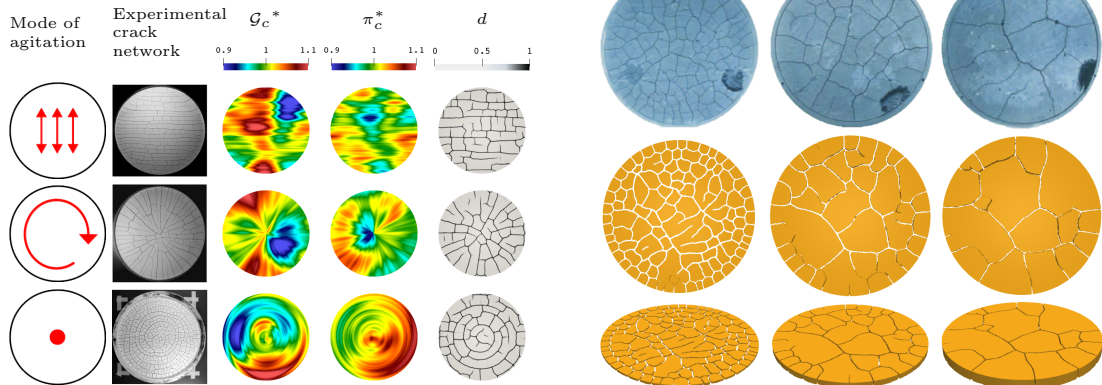
$\phi$  is a  $p$ -periodic function taken as

$$\phi(\tau; L) = \begin{cases} \frac{|\sin(\pi\tau/p)|}{L}, & (\text{Periodic Exponential, PE}), \\ \frac{\sin(\pi\tau/p)^2}{L^2}, & (\text{Periodic Squared-Exponential, PSE}). \end{cases} \quad (4)$$

Sensitivity to the correlation length  $L$ 

Sensitivity to  $\mathcal{G}_c$  and  $\pi_c$ 

### Flexibility of the stochastic model



Past work

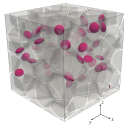
Soil Desiccation

Intergranular Fracture in UO<sub>2</sub>

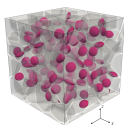
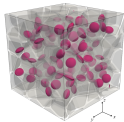
Preliminary results and findings

Towards ductile fracture

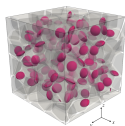
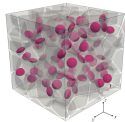
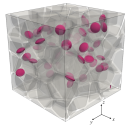
References



- ▶ A set of random close-packing (RCP) voronoi structures are realized by Maximal Poisson-disk Sampling (MPS).
- ▶ The polycrystalline microstructure is described by a set of non-conserved order variables  $\{\phi_i\}$  in a diffuse manner.
- ▶ The microstructure follows from a phase-field grain growth model [1].
- ▶ The grain boundaries are identified by  $\sum_i \phi_i^2 \geq 0.75$ .
- ▶ Gas bubbles are represented by another phase variable  $\phi_0$  and are uniformly distributed along grain boundaries, overriding existing order variables. The effect of gas pressure inside bubbles is neglected.

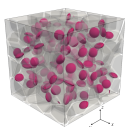
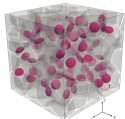
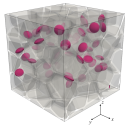


See [intergranular.pdf](#) for details.



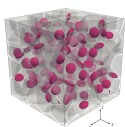
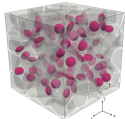
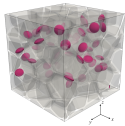
- ▶ A set of random close-packing (RCP) voronoi structures are realized by Maximal Poisson-disk Sampling (MPS).
- ▶ The polycrystalline microstructure is described by a set of non-conserved order variables  $\{\phi_i\}$  in a diffuse manner.
- ▶ The microstructure follows from a phase-field grain growth model [1].
- ▶ The grain boundaries are identified by  $\sum_i \phi_i^2 \geq 0.75$ .
- ▶ Gas bubbles are represented by another phase variable  $\phi_0$  and are uniformly distributed along grain boundaries, overriding existing order variables. The effect of gas pressure inside bubbles is neglected.
- ▶ A phase-field brittle fracture model is used.
- ▶ Grain boundaries have an arbitrarily high fracture toughness to facilitate intergranular fracture, i.e.  $\mathcal{G}_c^{\text{bnd}} \gg \mathcal{G}_c^{\text{grain}}$ .

See [intergranular.pdf](#) for details.



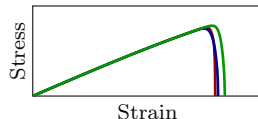
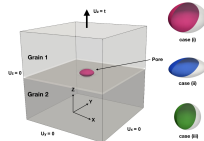
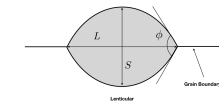
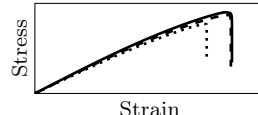
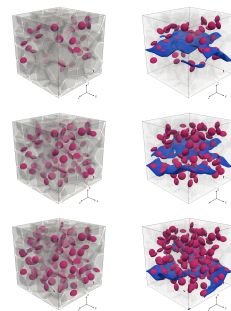
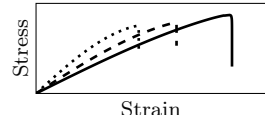
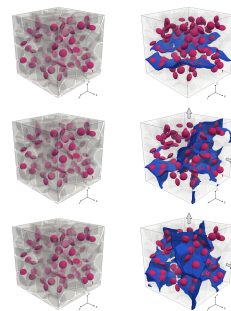
- ▶ A set of random close-packing (RCP) voronoi structures are realized by Maximal Poisson-disk Sampling (MPS).
- ▶ The polycrystalline microstructure is described by a set of non-conserved order variables  $\{\phi_i\}$  in a diffuse manner.
- ▶ The microstructure follows from a phase-field grain growth model [1].
- ▶ The grain boundaries are identified by  $\sum_i \phi_i^2 \geq 0.75$ .
- ▶ Gas bubbles are represented by another phase variable  $\phi_0$  and are uniformly distributed along grain boundaries, overriding existing order variables. The effect of gas pressure inside bubbles is neglected.
- ▶ A phase-field brittle fracture model is used.
- ▶ Grain boundaries have an arbitrarily high fracture toughness to facilitate intergranular fracture, i.e.  $\mathcal{G}_c^{\text{bnd}} \gg \mathcal{G}_c^{\text{grain}}$ .
- ▶ Numerical studies are performed to investigate the effect of bubble geometry, porosity and loading conditions on the fracture strength.

See [intergranular.pdf](#) for details.



- ▶ A set of random close-packing (RCP) voronoi structures are realized by Maximal Poisson-disk Sampling (MPS).
- ▶ The polycrystalline microstructure is described by a set of non-conserved order variables  $\{\phi_i\}$  in a diffuse manner.
- ▶ The microstructure follows from a phase-field grain growth model [1].
- ▶ The grain boundaries are identified by  $\sum_i \phi_i^2 \geq 0.75$ .
- ▶ Gas bubbles are represented by another phase variable  $\phi_0$  and are uniformly distributed along grain boundaries, overriding existing order variables. The effect of gas pressure inside bubbles is neglected.
- ▶ A phase-field brittle fracture model is used.
- ▶ Grain boundaries have an arbitrarily high fracture toughness to facilitate intergranular fracture, i.e.  $\mathcal{G}_c^{\text{bnd}} \gg \mathcal{G}_c^{\text{grain}}$ .
- ▶ Numerical studies are performed to investigate the effect of bubble geometry, porosity and loading conditions on the fracture strength.

See [intergranular.pdf](#) for details.

**Effect of bubble geometry****Effect of porosity****Effect of loading direction**

Past work

Soil Desiccation

Intergranular Fracture in UO<sub>2</sub>

Preliminary results and findings

Towards ductile fracture

References

Past work

Soil Desiccation

Intergranular Fracture in UO<sub>2</sub>

Preliminary results and findings

Towards ductile fracture

References

The free energy takes the following form

$$\pi(\mathbf{F}, \mathbf{F}^p, \bar{\varepsilon}^p, d, \nabla d) = \pi_{\text{elastic}}(\mathbf{F}, \mathbf{F}^p, d) + \pi_{\text{plastic}}(\bar{\varepsilon}^p, d) + \pi_{\text{fracture}}(d, \nabla d). \quad (5)$$

The elastic energy is defined as

$$\pi_{\text{elastic}}(\mathbf{F}, \mathbf{F}^p, d) = g^e(d) \pi_{\text{elastic}}^{(A)}(\mathbf{F}, \mathbf{F}^p) + \pi_{\text{elastic}}^{(I)}(\mathbf{F}), \quad (6a)$$

$$\pi_{\text{elastic}}^{(A)}(\mathbf{F}, \mathbf{F}^p) = H(J - 1) \left[ \frac{1}{2} K_s \left( \frac{1}{2}(J^2 - 1) - \ln J \right) \right] + \frac{1}{2} \mu_s (\bar{\mathbf{C}} : \mathbf{C}^{p-1} - 3), \quad (6b)$$

$$\pi_{\text{elastic}}^{(I)}(\mathbf{F}) = H(1 - J) \left[ \frac{1}{2} K_s \left( \frac{1}{2}(J^2 - 1) - \ln J \right) \right]. \quad (6c)$$

The plastic energy is defined as

$$\pi_{\text{plastic}}(\bar{\varepsilon}^p) = g^p(d) \sigma_Y \bar{\varepsilon}^p + g^h(d) \frac{1}{2} h \bar{\varepsilon}^{p2}. \quad (7)$$

See [hyperelasticity.pdf](#) for other hyperelastic potentials with tension-compression asymmetry.  
See [plasticity.pdf](#) for a detailed derivation.

Balance laws and constitutive equations:

$$\nabla \cdot \mathbf{P} + \rho_0 \mathbf{B} = \mathbf{0}, \quad (8)$$

$$-\nabla \cdot \boldsymbol{\pi}, \nabla d + \boldsymbol{\pi}, \dot{d} \geq 0, \quad \dot{d} \geq 0, \quad (9)$$

$$\rho_0 r - \pi_{,\bar{\varepsilon}^p} \dot{\bar{\varepsilon}}^p - \pi_{,d} \dot{d} = \rho_0 c \dot{T}, \quad (10)$$

The constitutive relation between the Kirchhoff stress and the deformation gradient is

$$\boldsymbol{\tau} = \mathbf{g}^e(\mathbf{d}) \boldsymbol{\tau}^{(A)} + \boldsymbol{\tau}^{(I)}, \quad (11a)$$

$$\boldsymbol{\tau}^{(A)} = \frac{1}{2} H(J-1) K_s (J^2 - 1) \mathbf{I} + \mu_s \operatorname{dev}(\mathbf{b}^e), \quad (11b)$$

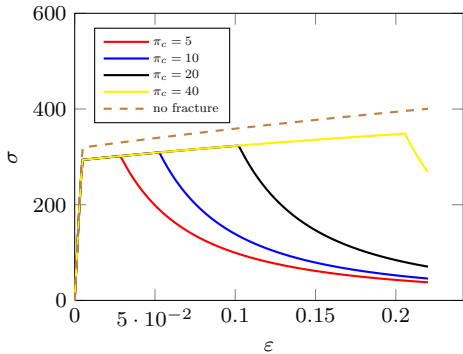
$$\boldsymbol{\tau}^{(I)} = \frac{1}{2} H(1-J) K_s (J^2 - 1) \mathbf{I}. \quad (11c)$$

The Kuhn-Tucker loading/unloading conditions are

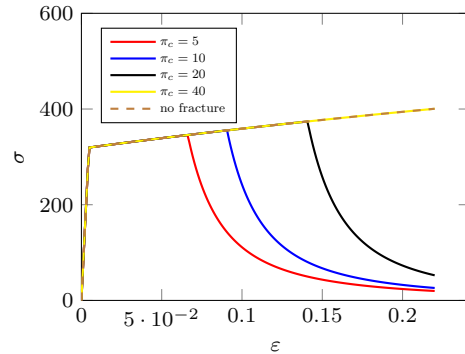
$$\phi(\mathbf{N}^p, \bar{\varepsilon}^p, d) = \|\operatorname{dev}(\boldsymbol{\tau})\| - \sqrt{\frac{2}{3}} \left[ \mathbf{g}^p(\mathbf{d}) \sigma_Y + \mathbf{g}^h(\mathbf{d}) h \bar{\varepsilon}^p \right] \leq 0, \quad \dot{\bar{\varepsilon}}^p \geq 0, \quad \dot{\bar{\varepsilon}}^p \phi(\mathbf{N}^p, \bar{\varepsilon}^p, d) = 0, \quad (12)$$

and the flow rule is

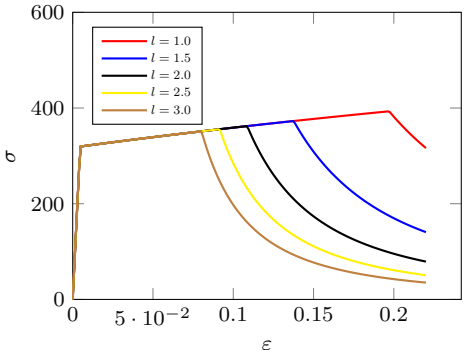
$$\dot{\mathbf{F}}^p \mathbf{F}^{p-1} = \dot{\bar{\varepsilon}}^p \mathbf{N}^p, \quad \mathbf{N}^p = \sqrt{\frac{3}{2}} \frac{\operatorname{dev}(\boldsymbol{\tau})}{\|\operatorname{dev}(\boldsymbol{\tau})\|}, \quad \det(\mathbf{F}^p) = 1. \quad (13)$$

Unperturbed elastic-plastic behavior

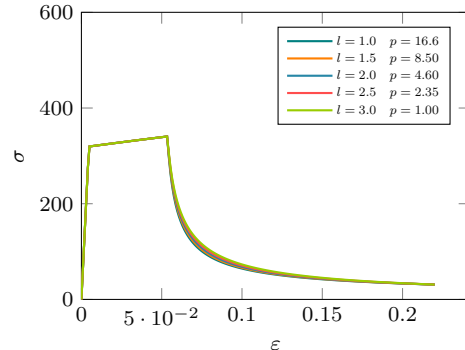
(a)



(b)

Regularization length-insensitive fracture strength

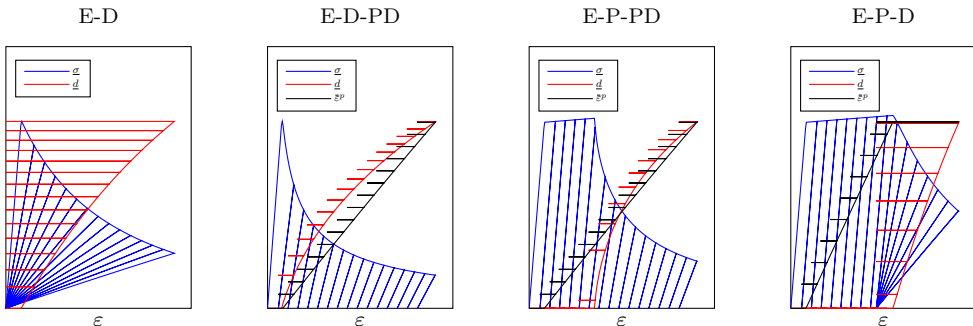
(a)



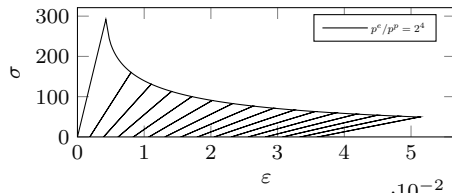
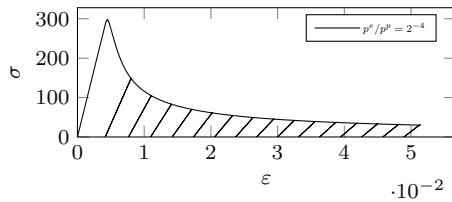
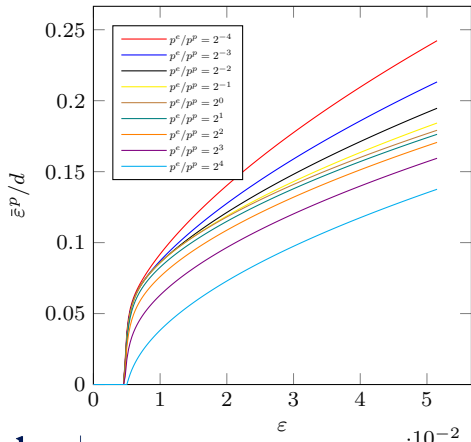
(b)

Following Alessi et. al. there are four representative stages.

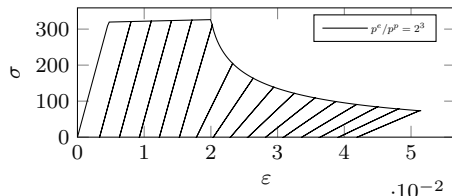
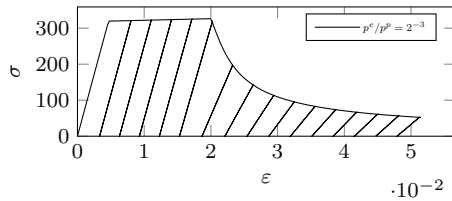
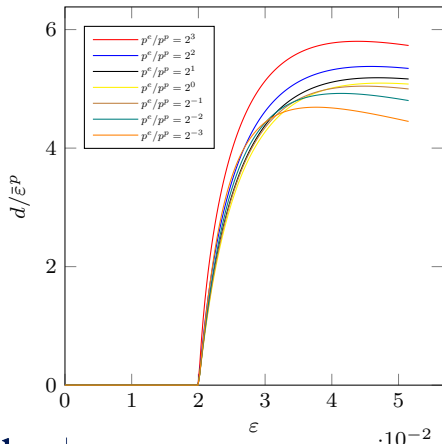
- ▶ E: elastic loading
- ▶ D: damage softening
- ▶ P: plastic hardening
- ▶ PD: mix of plastic hardening and damage softening



The shapes of the degradation functions (in particular, their derivatives) determine the amount of plastic dissipation during the damage softening process. **The E-D process may be viewed as a limiting case of the E-D-PD process.** Similarly, the E-P-D process may be viewed as a limiting case of the E-P-PD process.



The shapes of the degradation functions (in particular, their derivatives) determine the amount of plastic dissipation during the damage softening process. The E-D process may be viewed as a limiting case of the E-D-PD process. Similarly, the E-P-D process may be viewed as a limiting case of the E-P-PD process.



Dugdale's model and Barenblatt's model lead to different crack paths in a three-point bending problem.

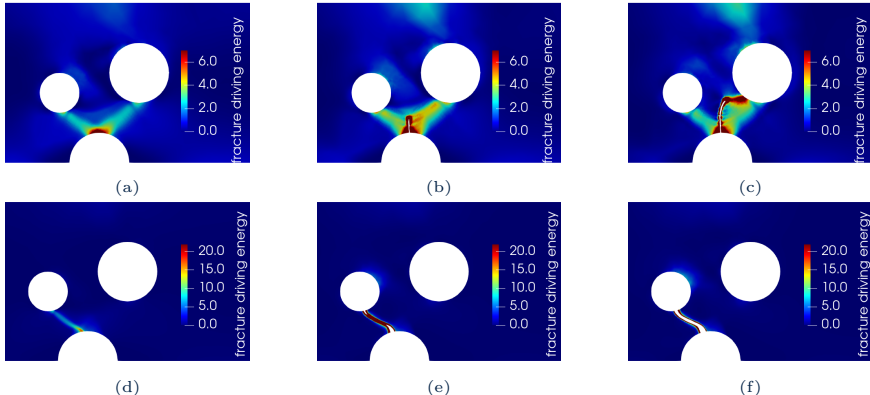


Figure: Contour plots of the total fracture driving energy  $\pi_{\text{elastic}}^{(A)} + \pi_{\text{plastic}}$  for (a-c) Dugdale's cohesive model and (d-f) Barenblatt's cohesive model.

-  N. Moelans, B. Blanpain, and P. Wollants.  
Quantitative analysis of grain boundary properties in a generalized phase field model for grain growth  
in anisotropic systems.  
*Phys. Rev. B*, 78:024113, Jul 2008.